


ORIGINAL RESEARCH

Rotational freedom thin-film solar cell using a reconfigurable nano-antenna with 4-Dimethyl-Amino-N-methyl-4-Stilbazolium Tosylate

Mohammad Ali Shamehli¹ | Mohammad Reza Eskandari²  | Reza Safian³¹School of Electrical and Computer Engineering, University of Tehran, Tehran, Iran²Department of Electrical Engineering, Shahreza Campus, University of Isfahan, Isfahan, Iran³imec USA, Kissimmee, Florida, USA**Correspondence**

Mohammad Reza Eskandari, Department of Electrical Engineering, Shahreza Campus, University of Isfahan, Isfahan, Iran.

Email: m.r.eskandari@shr.ui.ac.ir**Abstract**

In this paper, we proposed a new method to realize the rotational freedom of thin-film solar cells. In this method, an array of reconfigurable nano-patches fed by a plasmonic waveguide is integrated inside the solar cell to receive and trap light in the active layer. The reconfigurable nano-antenna is designed to achieve beam steering by bias voltage in the direction of sunlight during the day using 4-Dimethyl-Amino-N-methyl-4-Stilbazolium Tosylate as an active electro-optic material integrated into the plasmonic waveguide. The proposed solar cell is investigated using the finite-difference frequency-domain method and the drift-diffusion equations of COMSOL Multiphysics software at different wavelengths of light and a wide range of angles of incidence for transverse magnetic (TM) and transverse electric (TE) polarizations. The numerical results show increase in the absorption in large wavelengths of sunlight for the thin-film solar cell with nano-antenna, resulting in a short circuit current enhancement of 1.48 and 1.45 for TE and TM polarisations, respectively. Also, another advantage of the proposed reconfigurable structure is maintaining the performance in different angles of incidence, which may open up a new opportunity in solar energy harvesting.

KEYWORDS

metamaterial antennas, plasmonics, solar cells

1 | INTRODUCTION

Solar energy is the best candidate for solving the energy crisis, and environmental problems include increasing temperature and less significant rainfalls preventing carbon dioxide generation [1–3]. Recently, thin-film solar cells have attracted considerable attention due to their low cost, light-weight, and mechanically flexible ability [4–6]. However, the short optical path length of the photons leads to the low efficiency of solar cells [4–6]. In addition, changing the incident angle of sunlight during the day and in different seasons has doubled the problems of thin-film solar cells [7]. This important problem leads to using a mechanical rotator for the solar cell to tune the surface of the structures in the normal direction of the sunlight which causes increasing volume of the solar panels; thus designing a rotational freedom solar cell is one of the important demands of the photovoltaic cells [7].

In recent years, nanostructures have been applied to thin-film solar cells to trap sunlight and increase photo-current generation [8–21]. The nanostructures inside the solar cell increase the optical path length of photons leading to absorption enhancement. The nano-particles (nano-spheres, core-shell structures, nano-rods) at the thin-film solar cells trap sunlight inside the cells and enhance the electric field in the active layers [8–10]. Using metasurfaces as beam-formers [11, 12], lenses [13], and absorbers [14, 15] increase absorption of the thin-film solar cells. Directive nano-antennas integrated inside the solar cells could receive the visible light from the free space and improve the absorption [7, 16, 17]. The fractal structures trap sunlight at different wavelengths leading to near-unity absorption [18, 19]. The effects of incorporating the random distribution of silicon nano-spheres inside the solar cell to improve the performance of the solar cells and increase their efficiency have been investigated in

This is an open access article under the terms of the Creative Commons Attribution License, which permits use, distribution and reproduction in any medium, provided the original work is properly cited.

© 2022 The Authors. *IET Optoelectronics* published by John Wiley & Sons Ltd on behalf of The Institution of Engineering and Technology.

Refs. [20, 21]. It is shown that not only random distribution of nano-spheres has an easier fabrication, but also they can significantly improve the performance of the solar cell in comparison with periodic structures. Despite all these efforts, some drawbacks like plasmonic loss [7, 13], dependency on polarization [11, 12], and narrow bandwidth [11, 17] cause failure in the realization of an efficient solar cell. Another important disadvantage of thin-film solar cells is a dependency on the sunlight angle of incidence, which needs mechanical rotation during the day and in different seasons of the year [7, 13, 15–17].

The authors proposed a new architecture of thin-film solar cells with nano-antenna to enhance the efficiency of conventional cells without a mechanical rotator. The nano-antenna is the array of reconfigurable nano-patches fed by plasmonic waveguides. The dielectric layer of the plasmonic waveguide is 4-Dimethyl-Amino-N-methyl-4-Stilbazolium Tosylate (DAST) which is an important low loss electro-optic material due to the large susceptibility and high electro-optic coefficient [33] that is electrically tuned to make phase delayed leading to rotation of antenna beams and receive sunlight at different angles of incidence.

The electro-optic active materials are one of the best methods for real-time tuning optical devices through applying a bias voltage. Indium tin oxide (ITO) [22], $\text{Ge}_2\text{Sb}_2\text{Te}_5$ [23], liquid crystal [24] and VO_2 [25] are some active materials that could be used in polarisers [26], lenses [27], modulators [28], and also in beam-formers [29]. The other application of electro-optic materials is tuning the nano-antennas electrically with static structures [30–32]. In one case, the beam of semi-bowtie nano-antenna is steered by changing the conductivity of a parasitic graphene sheet [30]. Changing the radiation pattern of Yagi-Uda by tuning a thin layer of vanadium dioxide is another example of reconfigurable plasmonic nano-antenna [31]. In another structure, variation of the Fermi level energies of the graphene layer leads to tuning the direction of the plasmonic nano-antenna composed of Gold nano-rods [32].

Between the electro-optic active materials, DAST with negligible ohmic loss is the best choice for the application of solar energy [33]. Incorporating this material into the plasmonic waveguide, feeds the array of nano-patches and tunes the antenna beam at desirable angles through using different phase delays. Therefore, the proposed solar cell with the nano-antenna receives sunlight at different angles of incidence of sunlight. In the new architecture of this paper, we improve the performance of the thin-film solar cell with the reconfigurable array of nano-patches in terms of absorption and short circuit current. The enhancement of short circuit current is higher than other similar studies with the integrated nano-antennas inside the thin-film solar cells. Also, we realized the international demand for the rotational freedom solar cell using the reconfigurable nano-antenna. In other words, tuning the bias voltage of the structure leads to deviating the antenna beam to the direction of the sunlight without mechanical rotation. This is one of the most important advantages of the proposed structure that indicates the revolutionary progress of the solar cells.

2 | DESIGN AND ANALYSIS OF A TWO-ELEMENT ARRAY OF NANO-PATCHES ANTENNA FED BY PLASMONIC WAVEGUIDE

In this section, the reconfigurable nano-antenna will be designed and investigated with a full-wave simulation. Modelling the nano-antenna is realized in the transmit mode due to n equal behaviour to the receiver, based on the reciprocity theorem [34].

Figure 1 shows the schematic of the array of nano-patches with the dimensions of $W = 260$ nm and $L = 180$ nm, which is fed by the plasmonic waveguide. In this figure, the dielectric layer of the plasmonic waveguide, sandwiched between Ag and ITO, is made of Si_3N_4 and DAST. The larger thickness of the proposed dielectric layer leads to better interaction of plasmonic modes with the DAST, however, the side effect of increasing thickness is limiting the variation of the refractive index of the proposed dielectric layer. Therefore, choosing the thickness of 100 nm provides a proper variation for the refractive index and the interaction of plasmonic mode with DAST. The thickness of the ITO and Ag layer is set at 50 nm to confine plasmonic modes inside the core of the waveguide (see Figure 2a,b). Also, the thicknesses of the Si layer and substrate are $H_{\text{Si-Sub}} = 50$ nm and $H_{\text{ZnO-Sub}} = 220$ nm; The lengths of the first and second part of the waveguide with the width of $W_y = 20$ nm are designated $L_{x1} = 200$ nm and $L_{x2} = 900$ nm, based on parametric simulation. We design nano-antenna with a normal radiation pattern at a wavelength of 900 nm due to the low-performance of the thin-film solar cell between 700 and 1100 nm. A broadside beam is realized at the equal phase delay of two branches of the waveguide, feeding the nano-patches. Having the equal phase delay, DAST should have an equal refractive index as the Si_3N_4 with a refractive index of 2.45 [35]. The refractive index of DAST tuning by the bias voltage is calculated as:

$$n_i = n_0 + \frac{dn}{du} \left(\frac{V}{d_i} \right) \quad (1)$$

where d_i is the thickness of DAST, V is bias voltage, $n_0 = 2.2$ is the refractive index of the DAST at $V = 0$, and $dn/du = 3.41 \text{ nm/V}$ is the electro-optic coefficient. Based on Equation (1), setting the bias voltage at 6.45 V to the cores of the two branches of the waveguide leads to the equal refractive index and the normal radiation pattern of the nano-antenna.

The impedance of the nano-antenna should be matched to the plasmonic waveguide to have a minimum reflection. With the assumption of the negligible magnitude of the longitudinal term of the electric field in comparison with the transversal one, the transmission line model is applied to the structure [36], and the impedance of the nano-patch is calculated as [37].

$$Z_{\text{nano-patch}} = \frac{1}{Y_{in}} = \frac{1}{2G}, \quad (2)$$

$$G = \frac{W}{120\lambda_0} \left[1 - \frac{1}{24} \left(\frac{2\pi H_{\text{Core}}}{\lambda_0} \right)^2 \right],$$

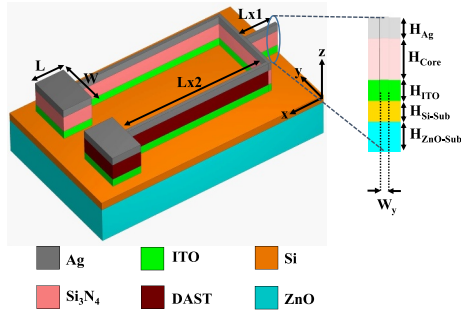


FIGURE 1 Schematic of the array of reconfigurable nano-patches fed by the plasmonic waveguide. The proposed waveguide has two branches with Si_3N_4 and 4-Dimethyl-Amino-N-methyl-4-Stilbazolium Tosylate DAST as dielectric layers with a thickness of $H_{\text{Core}} = 100$ nm, sandwiched between the Ag and the Indium tin oxide (ITO) layers, which have thicknesses of $H_{\text{Ag}} = 50$ nm and $H_{\text{ITO}} = 50$ nm. Also, the Si layer and substrate have thicknesses of $H_{\text{Si-Sub}} = 50$ nm and $H_{\text{ZnO-Sub}} = 220$ nm, respectively. The length of the first and second part of the waveguide with the width of $W_y = 20$ nm is $L_{x1} = 200$ nm and $L_{x2} = 900$ nm, respectively

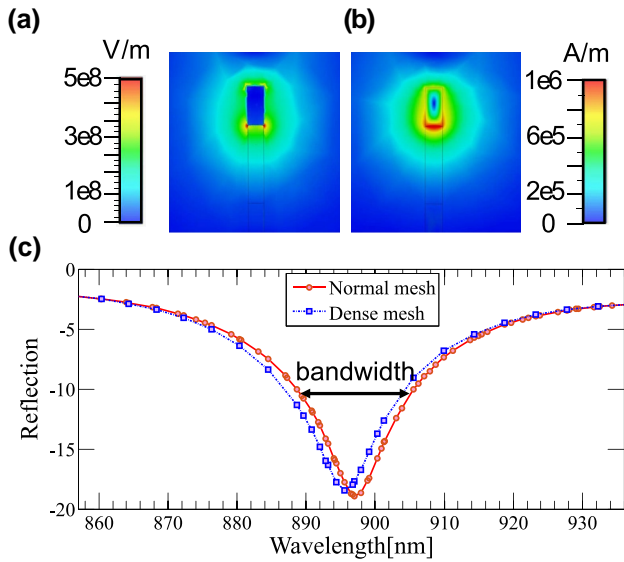


FIGURE 2 The numerically calculated magnitude of (a) the electric field and (b) the magnetic field of the cross-section of the plasmonic waveguide. (c) The reflection from the array of nano-patches fed by the plasmonic waveguide. The resonance dip around the wavelength of 900 nm represents the accurate design of the nano-antenna

where λ_0 is the wavelength of the free space, W is the width of the nano-patch, and H_{Core} is the thickness of the silicon nitride layer in the plasmonic waveguide (see Figure 1). Also, the characteristic impedance of the plasmonic waveguide feeding the nano-patch is calculated as [38].

$$Z_{PW} = \frac{Z_0}{n_{\text{eff}}}, \quad (3)$$

where $Z_0 = 377$ is the characteristic impedance of the free space and n_{eff} is the effective refractive index of the proposed plasmonic waveguide.

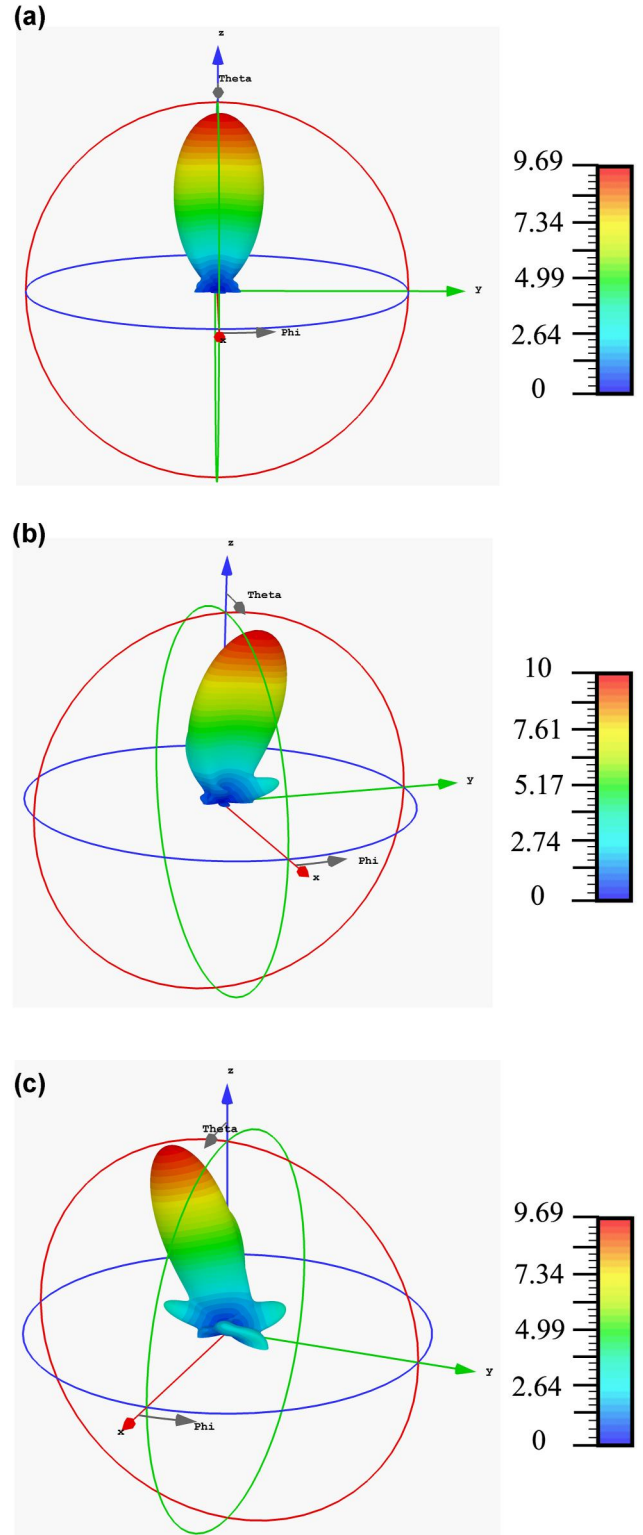


FIGURE 3 The numerically calculated radiation pattern at the direction of (a) normal angle at the bias voltage of $v_b = 6.45$ V, (b) $+20^\circ$ at the bias voltage of $v_b = 11$ V, and (c) -20° at the bias voltage of $v_b = -5.85$ V with a directivity around 10 in different states

In this step, we simulate the plasmonic waveguide in the CST using the finite-difference frequency-domain FDFD method with wave port excitation that propagates the

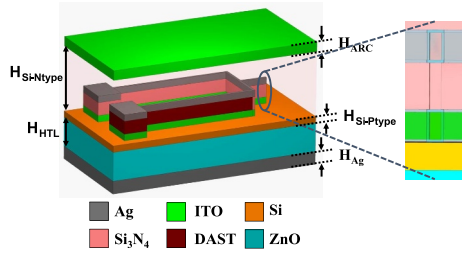


FIGURE 4 Schematic of the thin-film solar cell with the array of nano-patches. The hole transport layer, made of ZnO, has a thickness of $H_{HTL} = 220$ nm, and the active layer of the solar cell has a thickness of 350 nm ($H_{Si-Ptype} = 50$, $H_{Si-Ntype} = 300$). The anti-reflection layer, made of Indium tin oxide (ITO), has a thickness of $H_{ARC} = 75$ nm. Also, the thin layer surrounding the Ag and ITO layer at the cross-section of the waveguide is made of SiO_2 with a thickness of 5 nm preventing from dissipation of electrical current due to bias voltage

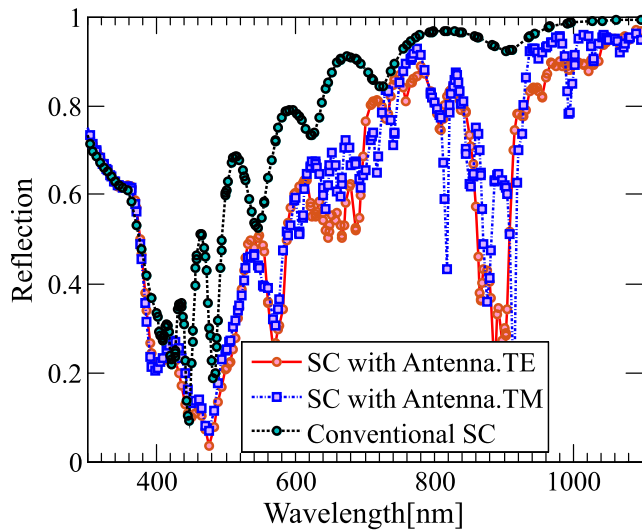


FIGURE 5 The reflection of the thin-film solar cell with the array of nano-patches in transverse electric (TE) and transverse magnetic (TM) polarisations and the conventional cell with an equal thickness of the active layer

plasmonic wave inside the waveguide between Ag and Si_3N_4 layers. One of the results of the proposed simulation is the effective refractive index of the waveguide, which is equal to 1.75, leading to the characteristic impedance of 215. In Figure 2a and b, the electric field and the magnetic field represents the plasmonic mode between the dielectric and Ag layer. Due to the matching with nano-antenna, the width of the nano-patch should be $W = 260$ nm, and the length of the nano-patch is set equal to the quarter wavelength of the plasmonic wave propagating in the proposed waveguide ($L = 180$ nm See Figure 1).

After determining the dimensions of the waveguide and nano-patch to achieve a minimum reflection, the nano-antenna has been investigated by the full-wave simulation with the FDFD method. In this simulation, the open boundary conditions are applied around the structure of the nano-antenna, and the wave port excitation propagates the plasmonic mode inside the core of the waveguide, which is made of DAST and Si_3N_4 .

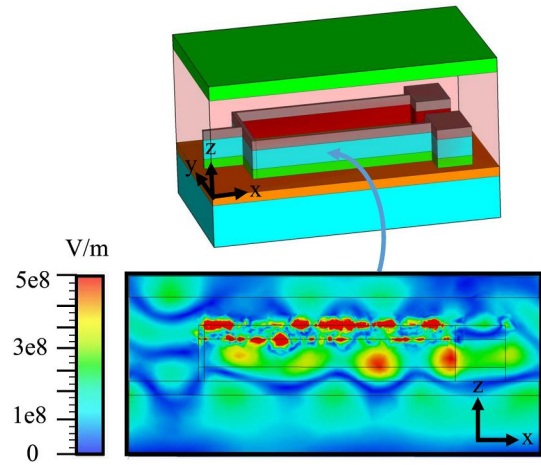


FIGURE 6 The magnitude of the electric field at the cross-section of the plasmonic waveguide (xz -plane), under the plane-wave illumination to the solar cell with transverse electric polarization for the wavelength of 900 nm. The electric field profile shows the propagation of the plasmonic mode in the proposed waveguide at the normal incidence of sunlight

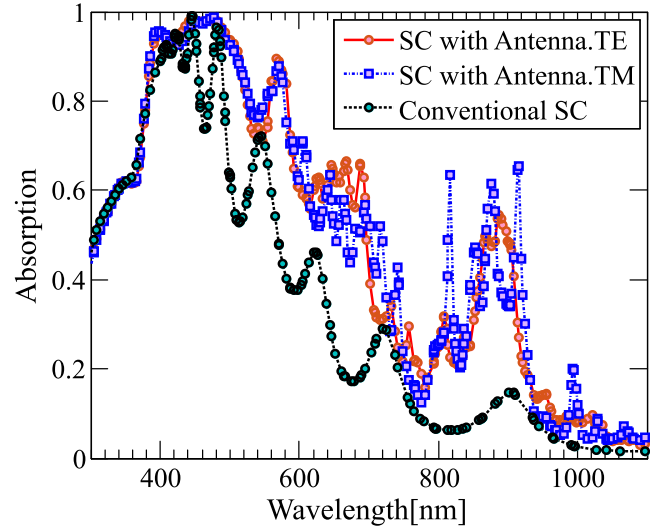


FIGURE 7 The absorption of the thin-film solar cell with the array of nano-patches in transverse electric (TE) and transverse magnetic (TM) polarisations, and the conventional cell with an equal thickness of the active layer

Also, the mesh size of the structure in our simulations is set automatically, with 38,581 meshes. Meshing automatically leads to defining a small mesh size for the plasmonic waveguide with thin dielectric and metallic layers and defining large mesh size for large areas, such as the substrate made of ZnO. Figure 2c shows the reflection of the array of nano-patches, matched with the plasmonic waveguide around the wavelength of 900 nm. As shown in this figure, increasing the mesh number of the FDFD simulation has a low impact on the reflection of the patch nano-antennas, however, the reflection dip slightly shifts to shorter wavelengths.

The radiation pattern is the other important characteristic of the nano-antenna, shown in Figure 3. In this figure, the directivity of the nano-antenna at the normal state is 10.5

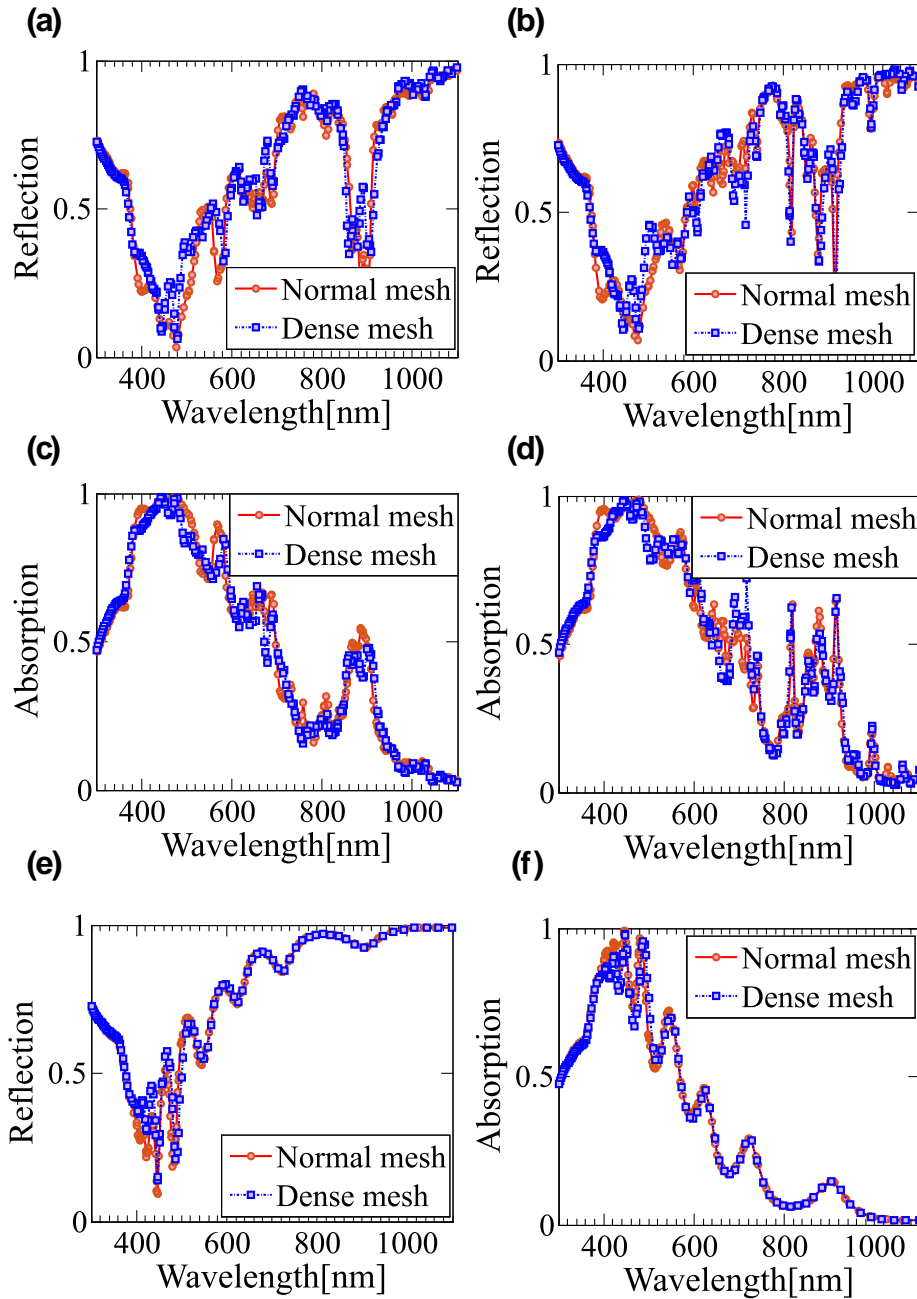


FIGURE 8 The reflection and absorption of the thin-film solar cell with the array of nano-patches in (a), (c) transverse electric and (b), (d) transverse magnetic polarisations, calculated by normal and dense mesh in the simulation process. (e) The reflection and (f) the absorption of the conventional cell with an equal thickness of the active layer for normal and dense mesh in the simulation process

(10.2 dB); the radiation efficiency of the nano-antenna, calculated by the FDFD method, is %71.

Changing the bias voltage of the DAST leads to the rotation of the antenna beam. As investigated, using a bias voltage of $v_b = 6.45$ V causes the refractive index of DAST to be equal to 2.45, the same as silicon nitride, and the radiation pattern stays at the normal state. Increasing bias voltage to 11 V leads to 20° deviation of the antenna beams (with directivity of 10). Also, on decreasing this parameter to $v_b = -5.85$ V, the antenna beam is placed at -20° (with directivity of 9.69) as shown in Figure 3c. Therefore, beam steering of the antenna is

realized by changing the bias voltage, and it could be integrated inside the thin-film solar cells to avoid mechanical rotation.

3 | NUMERICAL ANALYSIS OF THIN-FILM SOLAR CELL USING INFINITE ARRAYS OF PATCH NANO-ANTENNAS

In this section, we investigate the performance of the array of nano-patches integrated inside the thin-film solar cell. As shown in Figure 4, the nano-antenna is placed close to the

depletion layer (between the p -type and n -type layer) to enhance the electric field and separate electron-holes to reduce the recombination rate of the cell. The hole transport layer in this structure, made of ZnO with a thickness of $H_{HTL} = 220$ nm, is placed at the bottom of the active layer of the solar cell with a thickness of 350 nm ($H_{Si-Ptype} = 50$, $H_{Si-Ntype} = 300$). The ITO, as an anti-reflection coating, has a thickness of $H_{ARC} = 75$ nm, and the thin layer, which is surrounding the Ag and ITO layer at the cross-section of the waveguide, made of SiO₂ with a thickness of 5 nm, prevents

from dissipation of electrical current on applying the bias voltage. Also, the thin layer of SiO₂, as an insulator, surrounded the Ag and ITO layer of the waveguide (shown at the cross-section of the waveguide in Figure 4), prevents the dissipation of electrical current due to the bias voltage.

The proposed solar cell is simulated in the full-wave software with the FDTD method using periodic boundary conditions and the plane-wave excitation in the transverse electric (TE) and transverse magnetic (TM) polarisations. The periodic boundary conditions are realized by using the unit cell boundary of CST, and the excited first and second Floquet modes cause excitation of a plane-wave in TE and TM polarisations, respectively. To have a comprehensive investigation, we will compare the result of the proposed solar cell to the conventional cell with an active layer of 350 nm, and the results are depicted in Figures 5–10. The conventional SC is a simple solar cell without any antenna in the active layer of the structure. In other words, the active layer of the proposed conventional cell are simple bars of N- and P-type silicon with thicknesses of 300 and 50 nm, respectively.

The reflection of the proposed solar cell in TE and TM polarisations is depicted in Figure 5. As shown in this figure, the reflected sunlight from the solar cell with nano-antenna decreases in most wavelengths of light, representing the improvement of the proposed structure. Also, the reflection reduction around the wavelength of 900 nm shows the proper performance of the array of nano-patches in receiving sunlight. Figure 6 shows the electric profile of the cross-section of the solar cell with nano-antenna at the wavelength of 900 nm in TE polarisation. In this figure, the noteworthy enhancement of the electric field in the plasmonic waveguide is the sunlight received by nano-antenna. Also, an exciting local surface plasmon mode at the edge of the Ag layer causes absorption enhancement at this wavelength.

The absorption of the proposed structure is calculated as

$$A(\omega) = \frac{1}{2} \omega \text{Im}(\epsilon(\omega)) \int_v |E|^2 dv, \quad (4)$$

where $|E|$ is the electric field intensity, ω is the angular frequency, $\text{Im}(\epsilon(\omega))$ is the imaginary permittivity of silicon and

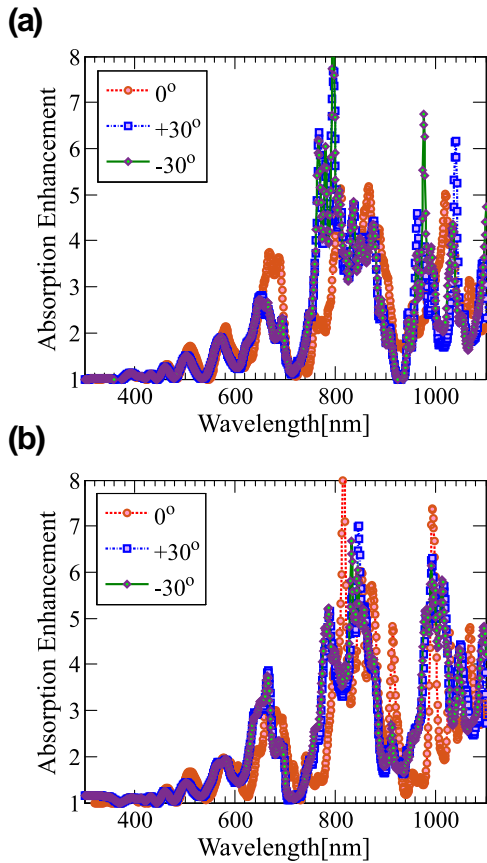


FIGURE 9 The absorption enhancement of the thin-film solar cell with the array of nano-patches in (a) transverse electric and (b) transverse magnetic polarisations, at the angles of 0°, +30°, and -30°

TABLE 1 Short circuit current and current enhancement of the proposed solar cell with the array of reconfigurable nano-patches compared to previous works

| Refs | Short circuit current (mA/cm ²) | Current enhancement | Nano-structure in the solar cell | Realization |
|-----------|---|---------------------|--|-------------|
| [7] | Not mentioned | 1.32 | Travelling nano-antenna | Simulation |
| [13] | Not mentioned | 1.18 | Metasurface lens | Simulation |
| [17] | Not mentioned | 1.39 | Spiral nano-antenna | Simulation |
| [40] | 12.26 | 1.22 | Micro-textured | Simulation |
| [41] | 13.90 | Not mentioned | Nano-needle antenna | Measurement |
| [42] | 12.50 | 1.26 | Nano-imprinted pattern | Measurement |
| [43] | 16.18 | 1.40 | Random nano-pattern | Measurement |
| This work | 16.13 | 1.46 | Array of reconfigurable patch nano-antenna | Simulation |

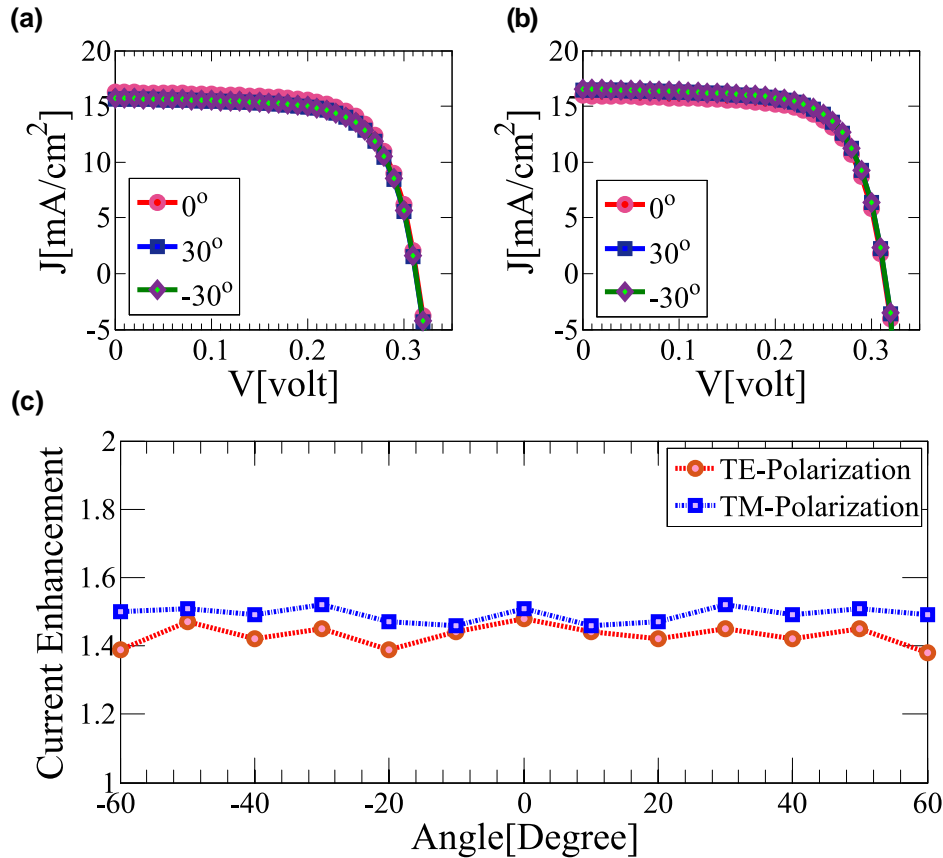


FIGURE 10 The IV curves of the thin-film solar cell with the array of nano-patches at 0° , $+30^\circ$, and -30° for (a) transverse electric (TE) and (b) transverse magnetic (TM) polarisations. (c) Current enhancement of the proposed solar cell in comparison with the conventional cell for TE and TM polarisations as a function of incident angle from -60° to 60°

the integral is taken in the active layer (silicon volume) [7]. Using Equation (4), the absorptions of the proposed structures in TE and TM polarisations are calculated and shown in Figure 7. As shown in this figure, the absorption of the proposed solar cell has improved with respect to the conventional cell, especially around wavelengths of 900 nm. This noteworthy enhancement represents the proper working of the nano-antenna. Also, exciting surface plasmonic mode between the Ag layer and silicon causes trapping of sunlight and improving absorption at the wavelength range of 550–750 nm. To validate the numerical results, which are calculated by the FDFD of CST software, we increase the mesh number in the simulation process. As shown in Figure 8, using dense mesh in the investigation of the thin-film solar cells leads to very little change, and both results calculated by normal and dense mesh have very good agreement with each other.

In the following, we investigate the performance of rotational freedom of the solar cell at different angles of the incidence. The advantage of free rotating structure realized by tuning the bias voltage leads to deviating the antenna beam to the direction of the sunlight and prevents reducing the performance of the thin-film solar cell at different angles of sunlight. In this section, we calculate absorption enhancement in 0° , 30° , and -30° by tuning the nano-antenna. As shown in Figure 9, the absorption of the proposed solar cell improved in most of the wavelengths of light and TE and TM polarisations.

Also, the performance of the proposed structure at different angles of incidence maintains at a good level representing the proper performance of the reconfigurable nano-antenna.

In the following, we electrically simulate the proposed structure using the Semiconductor module of the COMSOL based on the drift-diffusion equations. The doping of the p -type and n -type of the crystalline silicon layer is determined to be 10^{15} [1/cm³] based on parametric simulation, and the electron and hole mobility are assumed to be 1450 cm²/(V*s) and 500 cm²/(V*s). The electron affinity of silicon is set at 4.05 eV. The generation rate of the electron-hole in a solar cell is one of the important parameters in quantum efficiency, which is proportional to the absorption of incident photons. Here, we calculate the generation rates from the absorption of full-wave simulation of CST with the FDFD method, and then these values are imported to COMSOL. Also, the impact of recombination rate has been considered using lifetimes of $\tau_p = 500$ μ s and $\tau_n = 800$ μ s based on doping of the silicon layer [39]. The result of the simulation shows that the thin-film solar cell with nano-antenna has a short circuit current of 16.28 mA/cm² and 15.97 mA/cm², in TE and TM polarisations, respectively, while this parameter for the conventional cell is 11.01 mA/cm². This enhancement was realized by receiving sunlight with nano-antenna and excitation of plasmonic mode in the Ag and silicon layers. As another comparison, Table 1 compares the short circuit current and current

enhancement achieved in this work with those reported in the previous works. As shown in this table, the current enhancement achieved in this work is higher than the enhancement reported in the previous thin-film solar cells.

Figure 10a and b show the IV curves of the proposed solar cell at the incident angles of -30° , 0° , and 30° for both TE and TM polarisations. As shown in these figures, using the reconfigurable antenna with a rotational beam causes maintaining IV curve as the normal incidence angle. The current enhancement of the structure, shown in Figure 10c, represents the independence to the angles of incidence and the rotational freedom of the proposed solar cell, which is not necessary to the mechanical rotator. The important note is tuning the proposed reconfigurable nano-antenna integrated inside the thin-film solar cell by hand, however, for the final structure with optimum parameters, the tuning can be automatically at different times of the day and seasons.

4 | CONCLUSION

A new method was proposed to enhance the performance of thin-film solar cells. In this method, an array of reconfigurable nano-patches was integrated inside the solar cell to receive and trap sunlight in the active layer. The beam of the reconfigurable nano-antenna deviated in different directions of sunlight resulting in the realization of freedom rotational thin-film solar cell. The proposed structure was numerically analysed in a broad range of wavelengths as well as different angles of incidence and TM and TE polarisations. The numerical results showed that the proposed technique enhances light absorption in all wavelengths at the range of 300–1100 nm. This enhancement in large wavelengths is due to the reconfigurable nano-antenna that makes this structure unique among other thin-film solar cells. Also, the short circuit current enhancement in 0° of the incidence light was 1.48 and 1.45 for TE and TM polarisations, respectively.

ACKNOWLEDGEMENT

The authors received no financial support for this work.

CONFLICT OF INTEREST

No conflict of interest has been declared by the authors.

DATA AVAILABILITY STATEMENT

The data that support the findings of this study are available from the corresponding author upon reasonable request.

ORCID

Mohammad Reza Eskandari  <https://orcid.org/0000-0002-3819-378X>

REFERENCES

- Zhang, R., et al.: Influence of SiO₂ shell thickness on power conversion efficiency in plasmonic polymer solar cells with Au nanorod@ SiO₂ core-shell structures. *Sci. Rep.* 6, 1–9 (2016)
- Yu, P., et al.: Effects of plasmonic metal core-dielectric shell nanoparticles on the broadband light absorption enhancement in thin film solar cells. *Sci. Rep.* 7, 1–10 (2017)
- Olaïmat, M.M., Yousefi, L., Ramahi, O.M.: Using plasmonics and nanoparticles to enhance the efficiency of solar cells: review of latest technologies. *JOSA B.* 38, 638–651 (2021)
- Atwater, H.A., Polman, A.: Plasmonics for improved photovoltaic devices. *Nat. Mater.* 9, 205–213 (2010)
- Massiot, I., Cattoni, A., Collin, S.: Progress and prospects for ultrathin solar cells. *Nat. Energy.* 5, 959–972 (2020)
- Yan, W., et al.: Photocurrent enhancement for ultrathin crystalline silicon solar cells via a bioinspired polymeric nanofilm with high forward scattering. *Sol. Energy Mater. Sol. Cells.* 186, 105–110 (2018)
- Taghian, F., Ahmadi, V., Yousefi, L.: Enhanced thin solar cells using optical nano-antenna induced hybrid plasmonic travelling-wave. *J. Lightwave Technol.* 34, 1267–1273 (2016)
- Qin, P., et al.: Grain boundary and interface passivation with core-shell Au@ CdS nanospheres for high-efficiency perovskite solar cells. *Adv. Funct. Mater.* 30, 1908408 (2020)
- Kumar, K., et al.: Tandem organic solar cells containing plasmonic nanospheres and nanostars for enhancement in short circuit current density. *Opt. Express.* 27, 31599–31620 (2019)
- Xiong, J., et al.: Solution growth of BiSI nanorod arrays on a tungsten substrate for solar cell application. *ACS Sustain. Chem. Eng.* 8, 13488–13496 (2020)
- Shameli, M.A., Salami, P., Yousefi, L.: Light trapping in thin film solar cells using a polarization independent phase gradient metasurface. *J. Opt.* 20, 125004 (2018)
- Khan, M.R., et al.: Enhanced light trapping in solar cells with a metamirror following generalized Snell's law. *Opt. Express.* 22, A973–A985 (2014)
- Shameli, M.A., Yousefi, L.: Absorption enhancement in thin-film solar cells using an integrated metasurface lens. *JOSA B.* 35, 223–230 (2018)
- Pala, R.A., et al.: Omnidirectional and broadband absorption enhancement from trapezoidal Mie resonators in semiconductor metasurfaces. *Sci. Rep.* 6, 1–7 (2016)
- Shameli, M.A., Fallah, A., Yousefi, L.: Developing an optimized metasurface for light trapping in thin-film solar cells using a deep neural network and a genetic algorithm. *JOSA B.* 38, 2728–2735 (2021)
- Pahuja, A., Parihar, M.S., Kumar, V.D.: Performance enhancement of thin-film solar cell using Yagi-Uda nanoantenna array embedded inside the anti-reflection coating. *Appl. Phys. A.* 126, 1–7 (2020)
- Pahuja, A., Parihar, M.S., Kumar, V.D.: Investigation of Euler spiral nanoantenna and its application in absorption enhancement of thin film solar cell. *Opt. Quant. Electron.* 50, 1–11 (2018)
- Kazerooni, H., Khavasi, A.: Plasmonic fractals: ultrabroadband light trapping in thin film solar cells by a Sierpinski nanocarpet. *Opt. Quant. Electron.* 46, 751–757 (2014)
- Shameli, M.A., Yousefi, L.: Absorption Enhanced Thin-film Solar Cells Using Fractal Nano-structures. *IET Optoelectronics.* (2021)
- Yao, Y., et al.: Broadband light management using low-Q whispering gallery modes in spherical nanoshells. *Nat. Commun.* 3, 1–7 (2012)
- Shameli, M.A., Mirnaziry, S.R., Yousefi, L.: Distributed silicon nanoparticles: an efficient light trapping platform toward ultrathin-film photovoltaics. *Opt. Express.* 29, 28037–28053 (2021)
- Feigenbaum, E., Diest, K., Atwater, H.A.: Unity-order index change in transparent conducting oxides at visible frequencies. *Nano Lett.* 10, 2111–2116 (2010)
- Wuttig, M., Yamada, N.: Phase-change materials for rewriteable data storage. *Nat. Mater.* 6, 824–832 (2007)
- Li, S.Q., et al.: Phase-only transmissive spatial light modulator based on tunable dielectric metasurface. *Science.* 364, 1087–1090 (2019)
- Dicken, M.J., et al.: Frequency tunable near-infrared metamaterials based on VO₂ phase transition. *Opt. Express.* 17, 18330–18339 (2009)
- Masyukov, M., et al.: Optically tunable terahertz chiral metasurface based on multi-layered graphene. *Sci. Rep.* 10, 1–10 (2020)
- Li, H., et al.: Wide-angle beam steering based on an active conformal metasurface lens. *IEEE Access.* 7, 185264–185272 (2019)

28. Zhang, J., et al.: Active metasurface modulator with electro-optic polymer using bimodal plasmonic resonance. *Opt. Express*. 25, 30304–30311 (2017)
29. Shirmanesh, G.K., et al.: Dual-gated active metasurface at 1550 nm with wide (>300) phase tenability. *Nano Lett.* 18, 2957–2963 (2018)
30. Basiri, R., Aghazade-Tehrani, M., Zareian-Jahromi, E.: Beam steering of a terahertz semi bow tie antenna using parasitic graphene ribbons. *Plasmonics*. 15, 1313–1322 (2020)
31. Rahimi, E., Şendur, K.: Temperature-driven switchable-beam Yagi-Uda antenna using VO₂ semiconductor-metal phase transitions. *Opt Commun*. 392, 109–113 (2017)
32. Dong, Z., et al.: A tunable plasmonic nano-antenna based on metal-graphene double-nanorods. *Laser Phys. Lett.* 15, 056202 (2018)
33. Aalizadeh, M., et al.: Toward electrically tunable, lithography-free, ultra-thin color filters covering the whole visible spectrum. *Sci. Rep.* 8, 1–11 (2018)
34. Neiman, M.S.: The principle of reciprocity in antenna theory. *Proceedings of the IRE*. 31, 666–671 (1943)
35. Van Erven, A.J.M., et al.: Effects of different firing profiles on layer characteristics and passivation properties of industrial ETP deposited silicon nitride films. In: 19th European Photovoltaic Solar Energy Conference. Paris (2004)
36. Yousefi, L., Foster, A.C.: Waveguide-fed optical hybrid plasmonic patch nano-antenna. *Opt. Express*. 20, 18326–18335 (2012)
37. Balanis, C.A.: *Antenna Theory: Analysis and Design*. John Wiley & Sons (2015)
38. Pozar, D.M.: *Microwave Engineering*. John Wiley & Sons (2011)
39. Fossum, J.G., Lee, D.S.: A physical model for the dependence of carrier lifetime on doping density in nondegenerate silicon. *Solid State Electron*. 25, 741–747 (1982)
40. Lipovšek, B., Krč, J., Topič, M.: Optimization of microtextured light-management films for enhanced light trapping in organic solar cells under perpendicular and oblique illumination conditions. *IEEE J. Photovoltaics*. 4, 639–646 (2013)
41. Di Vece, M., et al.: Plasmonic nano-antenna a-Si: H solar cell. *Opt. Express*. 20, 27327–27336 (2012)
42. Ferry, V.E., et al.: Improved red-response in thin film a-Si: H solar cells with soft-imprinted plasmonic back reflectors. *Appl. Phys. Lett.* 95, 183503 (2009)
43. Ferry, V.E., et al.: Optimized spatial correlations for broadband light trapping nanopatterns in high efficiency ultrathin film a-Si: H solar cells. *Nano Lett.* 11, 4239–4245 (2011)

How to cite this article: Shameli, M.A., Eskandari, M. R., Safian, R.: Rotational freedom thin-film solar cell using a reconfigurable nano-antenna with 4-Dimethyl-Amino-N-methyl-4-Stilbazolium Tosylate. *IET Optoelectron.* 16(4), 179–187 (2022). <https://doi.org/10.1049/ote2.12069>